Inertial magnetic reconnection effects on the electron dynamics in a three-dimensional configuration

2012 J. Phys.: Conf. Ser. 401 012019

(http://iopscience.iop.org/1742-6596/401/1/012019)

Journal of Physics: Conference Series **401** (2012) 012019 doi:10.1088/1742-6596/401/1/012019

Inertial magnetic reconnection effects on the electron dynamics in a three-dimensional configuration

A Perona[1], D Borgogno[2], D Grasso[3,2]

[1] Centre for Fusion, Space and Astrophysics, University of Warwick, United Kingdom
[2] Dipartimento di Energia, Politecnico di Torino, Italy
[3] Istituto Sistemi Complessi - CNR, Roma, Italy

Abstract. The three-dimensional response of a population of thermal electrons to a collisionless magnetic reconnection process is investigated through a relativistic Hamiltonian guiding centre formulation of the particle dynamics. The resulting electron equations have been implemented in a test-particle code that evolves the spatial position and the velocity of the electrons according to the fields calculated by the numerical solutions of a two-fluid reconnection model. In particular, we consider here reconnection events triggered by single helicity perturbations. By following the evolution of the electron distribution function we can quantify the number of suprathermal electrons generated during the nonlinear phase of reconnection and observe how the increase in the electron energy deforms the moments of the electron distribution function with respect to the corresponding fluid quantities.

1. Introduction

One of the most characteristic features of magnetic reconnection is the conversion of part of the stored magnetic energy into heating of the plasma and particle acceleration. Energetic electrons have been observed in the diffusion region of the Earth's magnetotail [1, 2, 3, 4], as well as during solar flares by *in situ* space measurements [5, 6, 7, 8, 9] and indirectly by the γ-ray lines produced in the chromosphere and in the photosphere. Electron acceleration also occurs following the reconnection of the magnetic field during sawtooth oscillations or disruptions in laboratory Tokamak experiments [10, 11], where the electrons can acquire such energies as to pose a potential danger to surrounding surfaces when they are finally lost. Understanding what conditions control the particle acceleration efficiency during the reconnection process is therefore important. Depending on the plasma parameters, on the magnetic field topology and on the type of reconnection, in fact, the energy distribution rate from magnetic field energy to the plasma particle energy can vary significantly.

In the past, test particles investigations of the effects produced on the thermal electrons populating the reconnection region have been carried out by adopting either analytically prescribed fields [12, 13, 14, 15], or the output of self-consistent magnetohydrodynamic (MHD) simulations [16, 17, 18]. Some of these studies, in particular, have explored particle acceleration in the solar corona [19, 20], and in astrophysical plasmas [21] considering three-dimensional (3D) resistive MHD fields.

As these works have pointed out, the precise structure of the reconnection electric field is the determining factor of the energization process in the reconnection region. In our work, we have

reconstructed the behaviour of a population of thermal electrons during a 3D inertial magnetic reconnection process characterized by a strong longitudinal ('guide') magnetic field. Such a process is described by a two-fluid model, considering a rarefied, high temperature plasma where the finite electron mass, and not the collisions between ions and electrons, can account for the violation of the ideal conductivity [22]. We have expressed the electron dynamics in the presence of the reconnection fields through a set of equations, based on a relativistic Hamiltonian approach, that represents the extension to the 3D geometry of a previous model aimed at investigating the electron behaviour in two-dimensional (2D) configurations [18].
Differently from the 2D case, 3D magnetic reconnection effects introduce regions of magnetic field line stochasticity produced by the nonlinear coupling of initial unstable perturbations with different helicities [23]. The investigation of the particle dynamics in these chaotic regions will be possible by means of the numerical code where the equations of the electron model have been implemented. In this paper, however, we present the numerical results related to a single-helicity case, introduced in Section 2. Although depending on all three spatial coordinates, the single-helicity case is equivalent to a 2D mode after a proper coordinate rotation. This allows us to perform a first 3D numerical investigation with our newly developed tool and to compare the results with those provided by the 2D study described in Ref. [18]. The numerical results describing the electron response in the presence of the reconnection fields are presented in Section 3. Finally, in Section 4 these results are discussed and conclusions are drawn.

2. The two-fluid reconnection model

We consider a dissipationless model of magnetic reconnection in a plasma immersed in a strong and uniform magnetic field [22]. This model, where the electron inertia is the term responsible for the breaking and reconnection of the magnetic field lines, is particularly apt at describing magnetic reconnection events in laboratory and space plasmas, where the density and the temperature are such as to make the contribution of collisions negligible [24]. The three-dimensional evolution of the magnetic flux and of the stream function is described by two-fluid, quasineutral ion and electron equations characterized by two characteristic scale lengths in the form of constant parameters. The electrons skin depth, $d_e = \sqrt{m/(\mu_0 n e^2)}$, is associated with the electron inertia, while the sonic Larmor radius, $\rho_s = \sqrt{T_e M/(eB^2)}$, is defined in terms of the ion inertia, M, and of the electron temperature, T_e. Ion temperature effects are neglected. The magnetic field, $\mathbf{B} = B_0 \mathbf{e}_z + \mathbf{e}_z \times \nabla\psi$, is expressed through the magnetic flux, $\psi = \psi(x, y, t)$, and has a strong constant guide field component, B_0, along z. The resulting equations, normalized to the macroscopic scale length, L, and to the Alfven time, $\tau_A = \sqrt{nM}L_x/B_{y0}$, with B_{y0} the characteristic magnitude of the equilibrium magnetic field, are

$$\frac{\partial F}{\partial t} + [\phi, F] - \rho_s^2 [U, \psi] = \frac{\partial \phi}{\partial z} - \rho_s^2 \frac{\partial U}{\partial z}, \tag{1}$$

$$\frac{\partial U}{\partial t} + [\phi, U] + [\psi, J] = - \frac{\partial J}{\partial z} \tag{2}$$

where $F = \psi + d_e^2 J$ is the generalized flux function, $U = \nabla^2 \phi$ is the vorticity, $J \equiv -\nabla^2 \psi$ is the current density and ϕ is the stream function, which in turn is related to the electrostatic potential Φ by the relation $\phi = (c/B_0)\Phi$.
The evolution of these fields is represented in a 3D slab geometry where magnetic curvature effects are not taken into account and periodic boundary conditions are imposed along the y and z directions. Vanishing boundary conditions and a non-uniform mesh with an increasing density of points in the reconnection region are assumed along x. The reconnection process is triggered by small amplitude, unstable reconnecting modes that are superimposed to the 'Harris pinch" equilibrium, $\psi_{eq} = -A \ln(\cosh(x))$, where the constant $A = 1$ represents the amplitude

of the equilibrium.
This 3D model can be traced back to the 2D limit when considering only one single-helicity (oblique) perturbation $\delta J(x,y,z;t) = -\nabla^2\delta\psi(x,y,z;t) = \hat{J}(x)exp(ik_y y + ik_z z)$, where $k_y = \pi m/L_y$ and $k_z = \pi n/L_z$ ($2L_y = 8\pi$ and $2L_z = 32\pi$ are the y- and z-sizes of the 3D box and (m,n) are the mode wave numbers along y and z). This single-helicity case, in fact, is equivalent to a two-dimensional mode after a proper coordinate rotation, $y_* = y + (k_z/k_y)z$. However, in the 3D representation of the single-helicity mode the equilibrium effective shear field is not symmetric with respect to the mode resonant surface. This causes a drift of the magnetic island with a velocity close to the fluid velocity at the magnetic X-point [23], while in the 2D case the magnetic island evolves on a rational surface coinciding with the position of the null line of the equilibrium sheared magnetic field. In our investigation we consider a collisionless reconnection process in the limit of the so-called large Δ regime ($\Delta\, d_e > min(1,(d_e/\rho_s))^{1/3}$ [25]), where Δ is the standard stability parameter of reconnection modes [26], recently extended to oblique modes [27]. This parameter depends on the analytical function describing the equilibrium magnetic flux. In particular, for the most unstable mode and for the (normalized) value of $d_e = 0.1682$ chosen for our study, we obtain $\Delta\, d_e \approx 1.26$.
The electric field parallel to the magnetic field lines can be expressed through the fields ψ and ϕ by remembering the relation that links the stream function to the electrostatic potential. As shown in Fig. 1, the parallel electric field exhibits a monopole structure peaked at the X-point of the magnetic island throughout the process, while it has an opposite sign along the separatrix of the island. In particular, during the nonlinear phase it is more negative along one arm of the separatrix than along the other, as an effect of the island asymmetry.

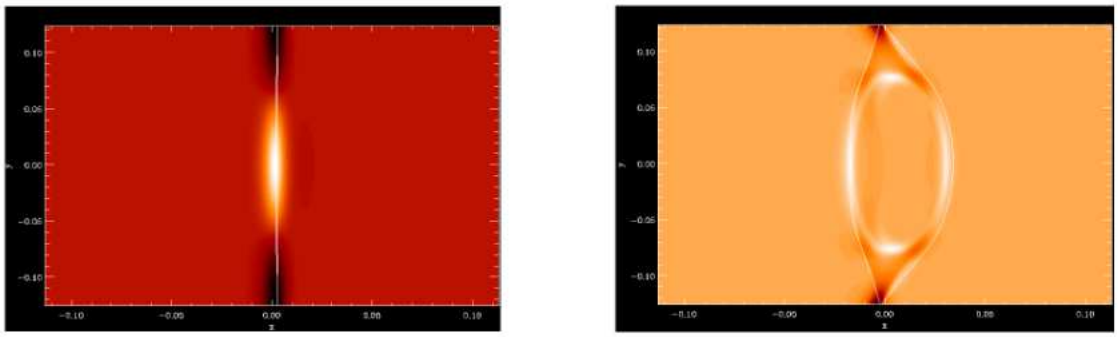

Figure 1. Contour levels in the (x,y) plane of the parallel electric field during the linear phase (left) and the nonlinear phase (right) of the reconnection process.

3. The electron response to the reconnection fields

In order to reconstruct the behaviour of the electrons in the presence of the reconnection fields we have derived a set of equations, based on a relativistic Hamiltonian formulation of the particle dynamics [28], which describes the evolution in time of the spatial position and of the parallel velocity of the electron guiding centres. These equations have been implemented in a numerical code that reads at each time step the reconnection fields calculated by a fluid code solving the magnetic reconnection equations introduced in Sec. 2. In order the electron dynamics to be coherent with the collisionless reconnection model considered in this paper, collisions have not been taken into account in the electron code. However, we have provided the code with a collisional operator reproducing their effect, which can be switched on when considering resistive models of magnetic reconnection characterized by longer time-scales.
After evaluating the reconnection fields in the whole reconnection region through a cubic spline

interpolation, the test electron code integrates the electron equations using a fourth-order Runge-Kutta method with adaptive stepsize control.
The evolution of the equilibrium Maxwellian electron distribution function and of its moments can be reconstructed at the end of each time step by considering the velocity and the spatial location of the particles at this step. However, this "*full-f*" approach produces effective results when the amplitude of the perturbation is large enough to overcome the background noise. For this reason, a δf technique has also been adopted in the code [29], which allows the small changes in the equilibrium quantities occurring during the linear phase of the process to be observed.
The fluid reconnection simulation considered in this work has been performed using a grid of 801× 128× 128 points and chosing the values of the two (normalized) parameters d_e and ρ_s in such a way as to correspond to those of typical fusion devices. Coherently, the test electron equilibrium density and temperature are initially taken as constant and uniform in the real space. Thus, simulations have been performed for $d_e = 0.1682 \cdot 10^{-2}$ m and $\rho_s = 0.3245 \cdot 10^{-2}$ m, corresponding to an equilibrium density $n_0 = 10^{19} \mathrm{m}^{-3}$ and an electron thermal temperature, $T_e \approx 1$ keV, respectively. As described in Fig. 2, after the initial transient, the reconnection process has a linear exponential behaviour between 60 τ_A and 180 τ_A, followed by a superexponential growth and a saturated state [30]. The results of the electron simulations have been obtained by reconstructing the dynamics of 10^7 particles in the reconnection region up to the end of the nonlinear phase.

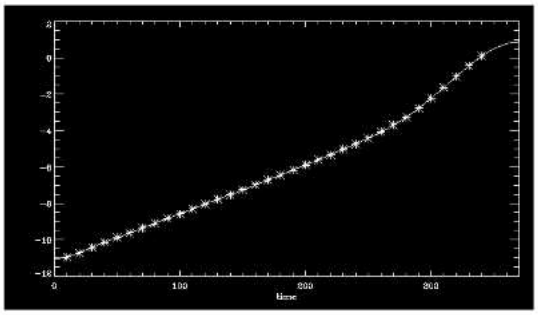

Figure 2. $\ln|\tilde{\psi}|$ evaluated at the X-point, vs the normalized time t/τ_A. The fluid fields are saved each 2 Alfvèn times. This choice represents the minimum sampling required in order to properly describe the electron dynamics. The stars represent up to which stage of the process the electron response has been reconstructed.

A good agreement characterizes the evolution of the moments provided by the electron simulations and the corresponding fluid quantities during the linear phase of the process. During the nonlinear phase, the parallel velocity of the electrons passing through the X-point increases, so that these particles move from the thermal bulk towards the tails of the electron distribution function. This acceleration affects the *parallel* electron temperature, $T_{\parallel e} \equiv p_{\parallel e}/n$, where n is the electron density and $p_{\parallel e}$ represents the longitudinal kinetic energy of the electrons.

Contrary to what expected by the isothermal closure of the fluid reconnection model, at this stage the temperature becomes significantly higher along the magnetic island separatrix with respect to the surrounding area and reaches the highest value in the denser regions, as shown in Fig. 3. In the following steps of the process, the number of the energized electrons becomes increasingly relevant, wherefrom a very significant distortion of the electron distribution function arises. The change with respect to the equilibrium Maxwellian distribution function at the end of the nonlinear phase is drawn in Fig. 4, taken at t=340 τ_A. At this time we can see that about 1/3 of the thermal electrons has run away from the original thermal bulk and that their velocity distribution generate a second Maxwellian centered at $v_{\parallel}/c = -0.15$.
In this mixed fluid-kinetic approach the electron response is not fed back to the fluid reconnection fields. A further development of the work that would allow us to reconstruct the process beyond the point at which the electron response and the fluid description do not agree any more

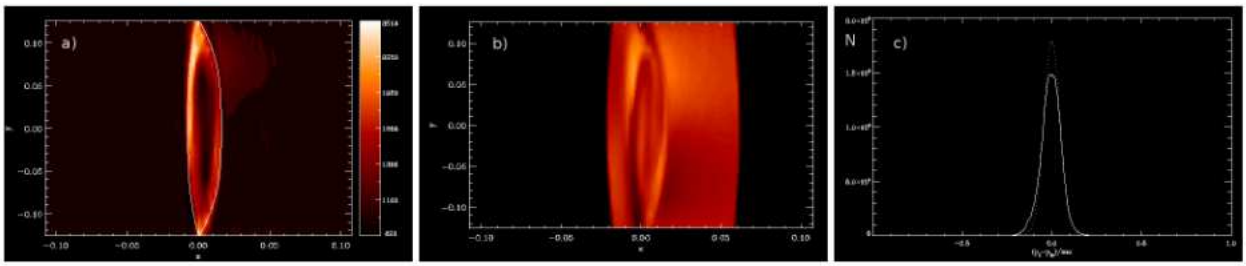

Figure 3. Contour levels in the (x, y) plane of the *parallel* electron temperature (a) and of the electron density (b) at t=320 τ_A. The white line represents the separatrix of the magnetic island. The distortion of the electron distribution function (continuous line) with respect to the equilibrium Maxwellian distribution function (dotted line) at this time is represented in Fig. (3c).

would consist in providing the fluid fields at each time step with the electron feedback, thus making the description of the process fully self-consistent.

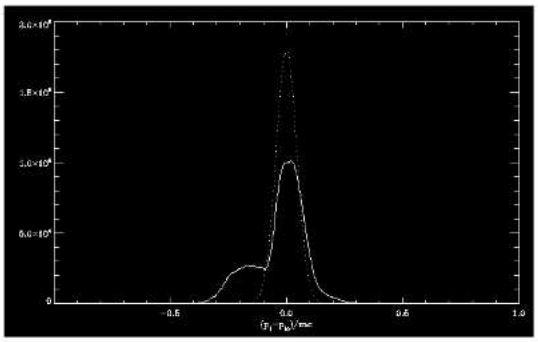

Figure 4. Distortion of the electron distribution function (continuous line) with respect to the equilibrium Maxwellian distribution function (dotted line) at the end of the nonlinear phase (t=340 τ_A). The shift of the non-thermal Maxwellian towards negative values of the velocity is due to the choice of a negative guide field component in the fluid simulations.

4. Discussion and conclusions

We have numerically investigated the effects of the fields characterizing an inertial magnetic reconnection process through a recently developed test particle code, which reproduces the dynamics of the electron guiding centres in a 3D cartesian geometry. As a first step, a single-helicity perturbation has been considered. Although this case is equivalent to a 2D mode, it still depends on all three spatial coordinates and is therefore useful for the validation of the correct behaviour of the 3D electron tool. Moreover, the fact that the single-helicity mode can be traced back to a 2D perturbation gives us the opportunity to compare the electron response with the one obtained in a previous investigation where the 2D version of the electron model had been used [18]. In that case, a fluid reconnection event described by the 2D version of Eqs. (1)-(2) had been studied with a different equilibrium function and a smaller equilibrium amplitude, $\psi_{eq} = 0.1/\cosh(x)^2$. Although the structure of the parallel electric field was still peaked at the X-point of the magnetic island throughout the process, similarly to the 3D electric field, no significant electron energization was observed and the electron response did not yield neither energetic nor relativistic tails in the distribution function. However, by the relation expressing the magnetic field configuration, $\mathbf{B} = B_0\mathbf{e}_z + \mathbf{e}_z \times \nabla\psi$, we know that the perpendicular component of the equilibrium magnetic field, $b_y = -\partial\psi_{eq}/\partial x$, depends on the equilibrium amplitude, A. The strong acceleration that we obtain in the 3D case can therefore be explained by

the large amount of magnetic energy that characterizes the reconnection process when $A = 1$. The strength of the perpendicular magnetic field naturally depends on the physical environment where magnetic reconnection occurs. In a Tokamak, for instance, the equilibrium amplitude that has been taken into account in this paper should be reduced in order to give a more realistic representation of the ratio of the toroidal to the poloidal component of the magnetic field also at the edge of the reconnection region. Then, it will be interesting to observe whether this choice still leads to a significant production of the highly energetic electrons experimentally observed during reconnection events in fusion devices. This aspect of the problem will be explored in the next step of our work.

References

[1] Oieroset M, Lin R P, Phan T D, Larson D E and Bale S D, Phys. Rev. Lett., **89**, 195001 (2002).
[2] Wang R-S, Lu Q-M, Guo J and Wang S, Chin. Phys. Lett., **25**, 3083 (2008).
[3] Vaivads A, Retinò A, Khotyaintsev Y V and Andre M, Ann. Geophys., **29**, 1917 (2011).
[4] Chen L-J, Bessho N, Lefebvre B, Vaith H, Asnes A, Santolik O, Fazakerley A, Puhl-Quinn P, Bhattacharjee A, Khotyaintsev Y, Daly P and Torbert R, Phys. Plasmas, **16**, 1056501 (2009).
[5] He J-S, Zong Q-G, Deng X-H, Tu C-Y, Xiao C-J, Wang X-G, Ma Z-W, Pu Z-Y, Lucek E, Pedersen A, Fazakerley A, Cornilleau-Wehrlin N, Dunlop M W, Tian H, Yao S, Tan B, Fu S-Y, Glassmeier K-H, Reme H, Dandouras I and Escoubet C P, Geophys. Res. Lett., **35**, L14104 (2008).
[6] Lin R P, Krucker S, Hurford G J, Smith D M, Hudson H S, Holman G D, Schwartz R A, Dennis B R, Share G H, Murphy R J, Emslie A G, Johns-Krull C and Vilmer N, The Ap. J., **595**, L69 (2003).
[7] Holman G D, Linhui S, Schwartz R A and Emslie A G, Astrophys. J., **595**, L97 (2003).
[8] Mann G and Warmuth A, A&A, **528**, A104 (2011).
[9] Vilmer N, Phil. Trans. R. Soc. A, **370**, 3241 (2012).
[10] Savrukhin P V, Phys. Rev. Lett., **86**, 3036 (2001).
[11] Klimanov I, Fasoli A, Goodman T P and the TCV team, Plasma Phys. Control. Fusion, **49**, L1 (2007).
[12] Heerikhuisen J, Litvinenko Y E and Craig I J D, ApJ, **566**, 512 (2002).
[13] Craig I J and Litvinenko Y E, ApJ, **570**, 387 (2002).
[14] Dalla S and Browning P K, A&A, **289**, 491 (2008).
[15] Sakai J, Sol. Phys., **140**, 99 (2002).
[16] Karlický M and Barta M, ApJ, **647**, 1472 (2006).
[17] Liu W J, Chen P F, Ding M D and Fang C, ApJ, **690**, 1633 (2009).
[18] Perona A, Eriksson L-G and Grasso D, Phys. Plasmas, **17**, 042104 (2010).
[19] Turkmani R, Cargill P J, Galsgaard K, Vlahos L and Isliker H, A&A, **449**, 749 (2006).
[20] Guo J-N, Büchner J, Otto A, Santos J, Marsch E and Gan W-Q, A&A, **513**, A73 (2010).
[21] Schopper R, Birk G T and Lesch H, Phys. Plasmas, **6**, 4318 (1999).
[22] Schep T J, Pegoraro F and Kuvshinov B N, Phys. Plasmas, **1**, 2843 (1994).
[23] Borgogno D, Grasso D, Porcelli F, Califano F, Pegoraro F and Farina D, Phys. Plasmas, **12**, 032309 (2005).
[24] Porcelli F, Borgogno D, Califano F, Grasso D, Ottaviani M and Pegoraro F, Plasma Phys. Control. Fusion, **44**, B389 (2002).
[25] Porcelli F, Phys. Rev. Lett., **66**, 425 (1991).
[26] Furth H P, Killeen J and Rosenbluth M N, Phys. Fluids, **6**, 459 (1963).
[27] Daughton W, Roytershteyn V, Karimabadi H, Yin L, Albright B J, Bergen B and Bowers K J, Nat. Phys., **7**, 539 (2011).
[28] Brizard A J and Chan A A, Phys. Plasmas **6** , 4548 (1999).
[29] Candy J, J. Comput. Phys. **129**, 160 (1996).
[30] Grasso D, Califano F, Pegoraro F and Porcelli F, Phys. Rev. Lett., **86**, 5051 (2001).